

# ALGEBRAIC MULTIGRID METHODS FOR VIRTUAL ELEMENT DISCRETIZATIONS: A NUMERICAL STUDY

DANIELE PRADA AND MICOL PENNACCHIO

**ABSTRACT.** We investigate the performance of algebraic multigrid methods for the solution of the linear system of equations arising from a Virtual Element discretization. We provide numerical experiments on very general polygonal meshes for a model elliptic problem with and without highly heterogeneous diffusion coefficients and we draw conclusions regarding the efficacy of the method.

## 1. INTRODUCTION

The high flexibility of polytopic grids is crucial when dealing with real life problems since it enables the treatment of complex geometries and simpler meshing of the domain including local mesh adaptivity and nonconforming grids without requiring any special treatment, e.g. for hanging nodes. This explains the increasing interest on numerical methods where the discretization is based on arbitrarily shaped polytopic meshes.

Here we focus on the Virtual Element Method (VEM) which is a quite recent PDE discretization method that allows for polygonal and polyhedral meshes and can be viewed as an extension of the Finite Element Method (FEM) [8, 10]. The name *virtual* is related to the fact that operators and matrices, needed in the implementation of the method, are evaluated by relying on an implicit knowledge of the local shape functions only, and are computed directly in terms of the degrees of freedom through a computable elementwise projector onto the space of polynomials.

The method has already been applied and extended to a wide variety of different model problems [45, 3, 4, 15, 16, 40, 27, 9, 32, 11, 18, 31]; the  $p$  and  $hp$  versions of the method are discussed and analyzed in [10, 5, 14, 39], its implementation can be found in [10] and its extension to the case of curved boundaries can be found in [17, 22].

In this paper we focus on the efficient solution of the linear system of equations associated with a VEM discretization of a model elliptic problem. The design of computationally effective solvers for such linear systems is a crucial phase of the overall numerical process. So far few works in literature have been devoted to the study of effective numerical algorithms for the solution of these linear systems of equations. Attempts in the recent literature focused on the increase in the condition number of the stiffness matrix due either to a degradation of the quality of the tessellation and/or to the increase in the polynomial order of the method [14, 38, 19]. Other works tackled the problem of the increase in the condition number resulting from refining the discretization by considering domain decomposition techniques [25, 24, 20, 41, 21] or  $p$  refinement multigrid methods [5].

We observe that designing geometric multigrid solvers for VEM for the case of  $h$  refinement is not straightforward. In fact, for such method, even if two grids are embedded one in the other, the two corresponding spaces are not. This makes the design of coarsening and prolongation operators tricky. The alternative is to use the algebraic version of multigrid. Algebraic multigrid (AMG) was introduced as a method for solving linear systems based on multigrid principles, without exploiting the problem geometry; only the connections in the matrix graph are used to determine intergrid

---

*Date:* December 6, 2018.

This paper has been realized in the framework of ERC Project CHANGE, which has received funding from the European Research Council (ERC) under the European Unions Horizon 2020 research and innovation programme (grant agreement No 694515).

transfer operators and to define coarse grids, see e.g. [42, 43]. AMG has already proved its usefulness in various problem types and especially those discretized on unstructured grids [26]. Here we want to exploit the performance of AMG solvers when very general polygonal meshes are considered, i.e. with very general shape as allowed by VEM.

AMG is also commonly used as a preconditioner for a Krylov subspace method such as the conjugate gradient (CG). The approach of using AMG with CG is often referred to as *CG accelerated multigrid (AMG/CG)* and it has the advantage that the Krylov method reduces the error in eigenmodes that are not being effectively reduced by multigrid.

The aim of this paper is to investigate the effectiveness of Algebraic Multigrid Methods (AMG) when applied to the linear system of equations associated with the lowest order VEM discretization. We follow the AMG/CG approach and analyze the performance of the conjugate gradient method implemented in PETSc [6] and its interfaces to different AMG preconditioners in the default setting. The interest in AMG techniques is mainly related to their potential scalability with the size of the problem to be solved, in the sense that the number of iterations required to reach convergence for a given problem does not depend on the number of the mesh nodes. The results of the present paper show that using AMG preconditioners for the solution of the linear system of equations associated with VEM discretizations is a promising approach, in terms of both scalability and reduction of the overall computational cost. With most of the meshes considered, AMG outperforms other classical solvers available in PETSc, in terms of computational times. However, we also verified that, when dealing with particularly complex and challenging meshes, not all the AMG preconditioners considered preserve scalability and those that do, loose most of their efficiency. The use of AMG/CG for the solution of linear systems associated with VEM discretization based on these meshes deserves further investigation, beyond the scope of this work.

The paper is organized as follows. The basic notation and the description of the Virtual Element Method are given in Section 2. Algebraic Multigrid Methods are briefly recalled in Section 3 with the different codes used. Numerical experiments to test the performance of AMG are presented in Section 4 and finally in Section 5 we draw conclusions on the efficiency and robustness of the AMG preconditioners considered.

## 2. THE VIRTUAL ELEMENT METHOD (VEM)

Let us start by recalling the definition and the main properties of the Virtual Element Method [8]. To fix the ideas we focus on the following model elliptic problem:

$$-\nabla \cdot (\rho \nabla u) = f \quad \text{in } \Omega, \quad u = 0 \quad \text{on } \partial\Omega,$$

with  $f \in L^2(\Omega)$  and  $\Omega \subset \mathbb{R}^2$  polygonal domain. We assume that the coefficient  $\rho$  is a scalar such that for almost all  $x \in \Omega$ ,  $\alpha \leq \rho(x) \leq M$  for two constants  $M \geq \alpha > 0$ . The variational formulation of such an equation reads as follows

$$(2.1) \quad \begin{cases} \text{find } u \in V := H_0^1(\Omega) \text{ such that} \\ a(u, v) = (f, v) \quad \forall v \in V \end{cases}$$

with

$$a(u, v) = \int_{\Omega} \rho(x) \nabla u(x) \cdot \nabla v(x) \, dx, \quad (f, v) = \int_{\Omega} f(x) v(x) \, dx.$$

We consider a family  $\{\mathcal{T}_h\}_h$  of tessellations of  $\Omega$  into a finite number of simple polygons  $K$ . The assumptions generally considered on each tessellation  $\mathcal{T}_h$  are the following (see, e.g. [8, 10]):

**Assumption 2.1.** there exist constants  $\gamma_0, \gamma_1, \alpha_0, \alpha_1 > 0$  such that:

- (1) each element  $K \in \mathcal{T}_h$  is star-shaped with respect to a ball of radius  $\geq \gamma_0 h_K$ , where  $h_K$  is the diameter of  $K$ ;

- (2) for each element  $K \in \mathcal{T}_h$  the distance between any two vertices of  $K$  is  $\geq \gamma_1 h_K$ ;  
 (3)  $\mathcal{T}_h$  is quasi-uniform, that is, for any two elements  $K$  and  $K'$  in  $\mathcal{T}_h$  we have  $\alpha_0 \leq h_K/h_{K'} \leq \alpha_1$ .

For simplicity we assume that for all  $K$  there exists a constant  $\rho_K$  such that the coefficient  $\rho$  verifies  $\rho = \rho_K$  on  $K$ . However, we remark that the virtual element method can also be defined for the case of coefficients varying within the elements of the tessellation, see e.g. [12].

The Virtual Element discretization space is defined element by element starting from the edges of the tessellation. More precisely, for each polygon  $K \in \mathcal{T}_h$  we introduce the space  $\mathbb{B}_1(\partial K)$  as

$$\mathbb{B}_1(\partial K) = \{v \in C^0(\partial K) : v|_e \in \mathbb{P}_1 \ \forall e \in \mathcal{E}^K\},$$

where  $\mathbb{P}_1$  denotes the set of polynomials of degree less than or equal to 1, and  $\mathcal{E}^K$  the set of edges of the polygon  $K$ . Letting

$$(2.2) \quad V_h^K = \{v \in H^1(K) : v|_{\partial K} \in \mathbb{B}_1(\partial K), \Delta v = 0 \text{ in } K\}$$

the discrete space  $V_h$  is then defined as

$$V_h = \{v \in V : w|_K \in V_h^K, \forall K \in \mathcal{T}_h\}.$$

Let  $(\cdot, \cdot)$  be the scalar product in  $L^2$ ,  $a(u, v) = (\rho \nabla u, \nabla v)$  and  $a^K$  the restriction of  $a$  to  $K$ . Using a Galerkin approach, we look for  $u_h \in V_h$  such that for all  $v_h \in V_h$

$$a(u_h, v_h) = \int_{\Omega} f v_h dx.$$

Both terms at the right and at the left hand sides cannot be computed exactly with the knowledge of the value of the degrees of freedom of  $u_h$  and  $v_h$  only. Setting, for each  $K \in \mathcal{T}_h$

$$a^K(u, v) = \int_K \rho \nabla u \cdot \nabla v$$

we observe that, by using Green's formula, given any  $v \in V_h^K$  and any  $p \in \mathbb{P}_1(K)$

$$a^K(p, v) = -\rho_K \int_K v \Delta p + \rho_K \int_{\partial K} v \frac{\partial p}{\partial n}.$$

Since on each edge of  $K$   $v$  is a known linear and  $\partial w/\partial n$  is a known constant, the right hand side can be computed exactly and directly from the degrees of freedom of  $v_h$ . This allows to define the “element by element” computable projection operator  $\Pi_K^\nabla : V_h^K \rightarrow \mathbb{P}_1(K)$

$$a^K(\Pi_K^\nabla u, q) = a^K(u, q) \quad \forall q \in \mathbb{P}_1(K),$$

and we clearly have

$$(2.3) \quad a^K(u, v) = a^K(\Pi_K^\nabla u, \Pi_K^\nabla v) + a^K(u - \Pi_K^\nabla u, v - \Pi_K^\nabla v).$$

The virtual element method stems from replacing the second term of the sum on the right hand side (which cannot be computed exactly), with an “equivalent” term, where the bilinear form  $a^K$  is substituted by a computable symmetric bilinear form  $S_a^K$ , resulting in defining

$$a_h^K(u, v) = a^K(\Pi_K^\nabla u, \Pi_K^\nabla v) + S_a^K(u - \Pi_K^\nabla u, v - \Pi_K^\nabla v).$$

As it is usually done in VEM, the bilinear form  $a$  is then replaced with a suitable approximate bilinear form  $a_h : V_h \times V_h \rightarrow \mathbb{R}$  defined by

$$a_h(u_h, v_h) = \sum_K a_h^K(u_h, v_h).$$

Different choices are possible for the bilinear form  $S_a^K$  (see [13]), the essential requirement being that it satisfies

$$(2.4) \quad c_0 a^K(v, v) \leq S_a^K(v, v) \leq c_1 a^K(v, v) \quad \forall v \in V_h^K \quad \text{with } \Pi_K^\nabla v = 0,$$

for two positive constants  $c_0$  and  $c_1$ , so that we have

$$(2.5) \quad (1 + c_0) a^K(v, v) \leq a_h^K(v, v) \leq (1 + c_1) a^K(v, v) \quad \forall v \in V_h^K,$$

and the local discrete bilinear forms satisfy the two following properties:

- *stability*:

$$(1 + c_0) a^K(v, v) \leq a_h^K(v, v) \leq (1 + c_1) a^K(v, v) \quad \forall v \in V_h^K,$$

- *consistency*: for any  $v_h \in V_h^K$  and  $p \in \mathbb{P}_1(K)$

$$(2.6) \quad a_h^K(v_h, p) = a^K(v_h, p).$$

In the numerical tests performed in Section 4 we made the standard choice of defining  $S_a^K$  in terms of the vectors of local degrees of freedom as the properly scaled euclidean scalar product.

As far as the linear form  $f$  on the right-hand side of the variational problem (2.1), it is discretized by  $f_h : V_h^K \rightarrow \mathbb{R}$  such that

$$f_h(v_h) := (\Pi_K^0 f, v_h)_{0,K} \quad \forall K \in \mathcal{T}_h,$$

where  $\Pi_K^0 : V_h^K \rightarrow \mathbb{R}$  denotes the  $L^2(K)$ -orthogonal projection onto constants, defined for any  $w_h \in V_h^K$  to be such that

$$\int_K (w_h - \Pi_K^0 w_h) dx = 0.$$

Thus the virtual element discretization of (2.1) yields the following discrete problem:

**Problem 2.2.** Find  $u_h \in V_h$  such that

$$a_h(u_h, v_h) = f_h(v_h) \quad \forall v_h \in V_h.$$

For the study of the convergence, stability and robustness properties of the method we refer to [8, 12].

**2.1. Matrix form.** We now focus on the construction of the linear system of equations stemming from problem 2.2. Proceeding as in the Finite Element Method (FEM), on each element, we consider a system of  $N$  shape functions,  $\{\varphi_i(\mathbf{x})\}_{i=1}^N$  associated with the  $N$  vertices of the element. We assume that the shape functions satisfy the Lagrange conditions, that is, they take value 1 at the vertex which they are associated with and zero at the other vertices. We deal with the standard basis for the space  $\mathbb{P}_K$  of local linear polynomials on each element  $K$ , that is, the set of scaled monomials of degree 1 that are defined on the element  $K$  as follows

$$(2.7) \quad \mathcal{M}_K := \left\{ m_1(x, y) := 1, \quad m_2(x, y) := \frac{x - x_K}{h_K}, \quad m_3(x, y) := \frac{y - y_K}{h_K} \right\},$$

with  $x_K, y_K$  and  $h_K$  being the barycenter and diameter of the element  $K$ , respectively.

If we write the virtual element solution  $u_h$  as  $u_h = \sum_{i=1}^N \text{dof}_i(u_h) \varphi_i$ , problem 2.2 can be rewritten in matrix form as

$$(2.8) \quad \mathbf{A} \mathbf{u} = \mathbf{f},$$

where the elements of matrix  $A$  and of  $\mathbf{f}$  are:

$$a_{j,i} = \sum_{K \in \mathcal{T}_h} (a_h^K(\nabla \Pi_K^\nabla \varphi_i, \nabla \Pi_K^\nabla \varphi_j) + \mathcal{S}^K(\varphi_i - \Pi_K^\nabla \varphi_i, \varphi_j - \Pi_K^\nabla \varphi_j)), \quad i, j = 1, \dots, N,$$

$$f_j = \sum_K (\Pi_K^0 f, \varphi_j)_{0,K}, \quad j = 1, \dots, N.$$

Both these terms are defined through sums over elements thus the virtual element method implementation is similar to that of a standard finite element method. The main difference with FEM is that the computation of the VEM local stiffness matrices relies on computing the local projector  $\Pi^K$  on each element first. Moreover, while the implementation of a finite element may rely on a mapping to a reference element, this is not possible in VEM because the mesh elements are allowed to be general polygons.

### 3. ALGEBRAIC MULTIGRID

Algebraic multigrid (AMG) was introduced as a method for mimicking the performance of geometric multigrid on unstructured grids. The multilevel process is realized from a purely algebraic standpoint without any explicit knowledge of the problem geometry. The most popular published implementation of the algorithm is the one by Ruge and Stuben (RS) [42]; for an introduction to AMG, see e.g. [23, 44, 30] and [47] for parallel AMG methods.

The two main components of multigrid are *smoothing* and *coarse-grid correction*. Coarse-grid correction involves operators that transfer information between fine and coarse “grids”, i.e., from the vector space  $\mathbb{R}^n$  to the coarse vector space  $\mathbb{R}^{n_c}$ . *Prolongation* maps the coarse grid to the fine grid and is just the matrix  $P : \mathbb{R}^{n_c} \rightarrow \mathbb{R}^n$ . *Restriction* maps the fine grid to the coarse grid and is the transpose of interpolation,  $P^T$ . The two-grid method for solving (2.8) is then:

```
do  $n_1$  smoothing steps on  $\mathbf{A}\mathbf{u} = \mathbf{f}$ .
Compute residual  $\mathbf{r} = \mathbf{f} - \mathbf{A}\mathbf{u} = \mathbf{A}\mathbf{e}$ .
Solve  $\mathbf{A}_c\mathbf{e}_c = P^T\mathbf{r}$ .
Correct  $\mathbf{u} \leftarrow \mathbf{u} + P\mathbf{e}_c$ .
do  $n_2$  smoothing steps on  $\mathbf{A}\mathbf{u} = \mathbf{f}$ .
```

The vector  $\mathbf{e} = A^{-1}\mathbf{f} - \mathbf{u}$  is the difference between the exact solution and the current iterate and it is called the *error*. The coarse system  $A_c\mathbf{e}_c = P^T\mathbf{r}$  is solved by re-applying the algorithm, yielding a hierarchy of coarse grids, transfer operators, and coarse-grid systems.

In the AMG method these components are realized in a purely algebraic way, without exploiting any knowledge of the underlying discretization method. The *smoother* (or relaxation process) is generally an iterative method such as point-wise Gauss-Seidel, which effectively eliminates some errors, while other components of the error are reduced quite slowly. The smooth error component, in the case of AMG, is then defined to be any component of the error not reduced by the relaxation. The nonzero structure of the matrix is used to determine the adjacency relationships between the unknowns and the smooth error components are related to strongly connected degrees of freedom. We say that  $u_i$  is connected to  $u_j$  if the element matrix  $a_{ij} \neq 0$ . The magnitude of  $a_{ij}$  indicates how strong the connection is and how much influence the error at  $j$  has on the error at  $i$  in the relaxation. Following the classic RS algorithm [42],  $u_i$  is defined to be strongly connected to  $u_j$  if  $-a_{ij} \geq \theta \max_{k \neq i} (-a_{ik})$ , with  $\theta$  being a user-defined strength threshold.

An alternative successful coarsening strategy is based on the so-called *smoothed aggregation* (SA) technique [46], where a coarse node is defined by an aggregate of a root point  $i$  and all the neighboring nodes  $j$  such that  $a_{ij} > \theta \sqrt{|a_{ii}a_{jj}|}$ .

The AMG algorithms have setup costs associated with the automatic selection of coarse grid operators that other multilevel methods do not have in general. This automatic selection makes implementing the algorithm into a given application simpler, but it does add extra computations to every simulation that cannot be a priori estimated.

In this work we follow the *CG accelerated multigrid* (AMG/CG) approach where AMG is used as a preconditioner for the conjugate gradient (CG) method. This approach has the advantage that

the Krylov method reduces the error in the eigenmodes that are not being effectively reduced by multigrid.

All our numerical experiments were carried out by using the Portable Extensible Toolkit for Scientific computation (PETSc) [6]. We now briefly recall the methods and the corresponding codes used for the numerical tests.

**3.1. Methods.** As iterative solvers, we used the conjugate gradient method implemented in PETSc [6] and its interfaces to different AMG preconditioners, with default settings. More precisely we considered:

- **GAMG:** native AMG preconditioner implemented in PETSc. We tested two different versions: a classical AMG method (c-GAMG) and a smoothed aggregation AMG method (a-GAMG) [7].
- **BoomerAMG:** a parallel algebraic multigrid solver and preconditioner, which is part of the *hypre* library [29] (<http://www.llnl.gov/CASC/hypre/>).
- **ML:** Multi Level Preconditioning Package, a smoothed aggregation algebraic preconditioner developed at Sandia National Laboratories [33] (<https://trilinos.org/packages/ml/>).

We also compared the performance of several direct solvers, which were called via the interfaces available in PETSc [6]:

- **SuperLU and SuperLU-Dist:** sparse LU codes developed by Jim Demmel, Xiaoye S. Li, and John Gilbert [37] (<http://crd-legacy.lbl.gov/~xiaoye/SuperLU/>);
- **UMFPACK:** part of the SuiteSparse package developed by Timothy Davis [28] (<http://www.cise.ufl.edu/research/sparse/>);
- **MUMPS:** MUltifrontal Massively Parallel sparse direct Solver, developed by Patrick Amestoy, Iain Duff, Jacko Koster, and Jean-Yves LExcellent [1, 2] (<http://www.enseeiht.fr/lima/apo/MUMPS/credits.html>);
- **PaStiX:** Parallel LU and Cholesky solvers [35] (<http://pastix.gforge.inria.fr/>).

SuperLU and UMFPACK are sequential solvers, whereas SuperLU-Dist, MUMPS, and PaStiX can handle distributed memory systems. These last three solvers were run using 2 processes.

All the experiments were run on a machine equipped with processor Intel<sup>®</sup> Core<sup>™</sup> i7-7820HQ, operating system Ubuntu Linux 16.04 LTS, memory 64GB, 2400MHz DDR4 Non-ECC SDRAM.

#### 4. NUMERICAL TESTS

In this section we present results for the solution of linear systems arising from the discretization with the virtual element method of degree one of the following model problem:

$$(4.1) \quad \begin{aligned} -\nabla \cdot (\rho \nabla u) &= f && \text{in } \Omega = (0, 1)^2, \\ u &= 0 && \text{on } \partial\Omega, \end{aligned}$$

with  $\rho$  diffusion coefficient. Boundary conditions and loading term are chosen so that  $u = \frac{1}{2\pi^2} \sin(2\pi x) \sin(2\pi y)$  is the exact solution. Several different meshes and diffusion coefficients  $\rho$  are considered. We start testing a constant-coefficient diffusion problem on a regular polygonal mesh, then we deal with irregular polygonal meshes, agglomeration of meshes and finally, highly heterogeneous coefficients  $\rho$ .

We analyze the performance of the Conjugate Gradient method (CG) preconditioned with different AMG preconditioners. All problems are run with different AMG codes but with fixed parameters.

Let  $\Omega$  and  $\mathcal{T}_h$  be the computational domain and a polygonal tessellation, respectively. We define:

- $N_{\text{elt}}$ , number of polygons of  $\mathcal{T}_h$ ,
- $N_{\text{v}}$ , number of vertices of  $\mathcal{T}_h$ .

- $h = \max_{K \in \mathcal{T}_h} h_K$ , where  $h_K$  is the diameter of element  $K \in \mathcal{T}_h$ .
- $h_{\min} = \min_{K \in \mathcal{T}_h} h_{\min,K}$ , where  $h_{\min,K}$  is the minimum distance between any two vertices of  $K$ .
- $\gamma_0 = \max_{K \in \mathcal{T}_h} \frac{h_K}{\rho_K}$ , where  $\rho_K$  is the radius of the largest ball that is contained inside  $K$ .
- $\gamma_1 = \max_{K \in \mathcal{T}_h} \frac{h_K}{h_{\min,K}}$ .

We consider different meshes by varying the shape of each cell and we study if the performance of the methods is affected by the shape of the cell and/or the presence of very small/large edges. We deal with the following different polygonal meshes  $\mathcal{T}_h$ :

- 1) regular hexagons meshes (Figure 1);
- 2) Voronoi meshes from uniformly random seed points (Figure 2);
- 3) meshes of "horse" cell (Figure 3); each horse is made up of 76 edges;
- 4) sequence of meshes obtained by embedding successive iterates of the Koch snowflake into a rectangle (Figure 4).

We remark that Voronoi and hexagonal meshes are the ones more likely to be used, whereas all the other meshes are considered here only for stress testing of AMG preconditioners. In particular we observe that snowflake meshes are particularly complex and challenging, as they are characterized by very small edges on the boundary of the snowflake and greater edges on the boundary of the square. These meshes may be of interest in domains with periodic structures.

Moreover, in view of a possible use of AMG in an adaptive approach, we also deal with meshes obtained by agglomerating an underlying fine mesh. More precisely, we consider different Voronoi and horse meshes and build coarse grid elements by agglomerating fine grid elements, that is, we deal with:

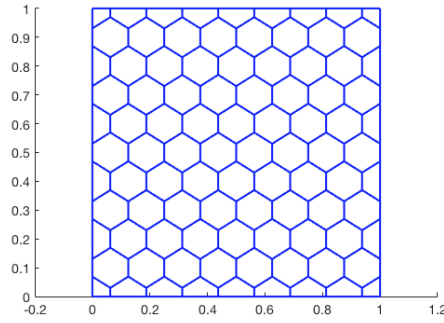
- 5) aggregates of Voronoi cells (Figure 5),
- 6) aggregates of "horse" cells (Figure 6).

Let us now analyze the results. The first Tables 1,3,5,9,11 list the values of the geometrical parameters defined above for each mesh considered; we recall that the number of unknowns coincides with the number of vertices  $N_v$ . Then, in Tables 2,4,6,8 and 10,12 (for the case of aggregates of cells), we report, for each mesh, the condition number  $\kappa$  of the matrix  $A$  in (2.8) with and without AMG preconditioning. The condition numbers are numerical approximations computed from the standard tridiagonal Lanczos matrix generated during the preconditioned CG iteration as the ratio between the maximum and the minimum eigenvalues, see e.g. [34]. Since in the following we deal also with a performance comparison of different (iterative and direct) solvers available in PETSc, the stopping criterion fixed for CG is defined by the relative residual error obtained with the direct solver SuperLU\_DIST (see `atol` reported in each Table).

We start by presenting the behavior of the condition number and of the iteration count when hexagonal meshes are taken into account. In this case the scalability of all the AMG preconditioners considered is clearly shown in Table 2: the iteration count to converge does not depend on the number of the mesh nodes. If we pass from hexagonal to Voronoi meshes (see Table 4), which are characterized by worse geometrical parameters, we notice only a slight increase in the number of iterations and in the condition number while the scalability is still preserved.

Instead, when dealing with horse or snowflake elements, we note an increase in the number of iterations (Tables 6-8); scalability is not preserved by c-GAMG. The best results are obtained by using BoomerAMG for the horse meshes and ML for the snowflake meshes. In this last case, scalability is preserved also by BoomerAMG and a-GAMG, but with a higher number of iterations. Similar results can also be observed with meshes of agglomerates of Voronoi or horse cells (see Tables 10 and 12). As before, BoomerAMG outperforms the other preconditioners, but, for the agglomerates

FIGURE 1. Hexagonal mesh

TABLE 1. Meshes of regular hexagons; for all these meshes,  $\gamma_0 \approx 5.33$ ,  $\gamma_1 \approx 3.16$ .

Mesh	$N_{\text{elt}}$	$N_v$	$h$	$h_{\text{min}}$
hexa <sub>1</sub>	10 151	20 304	$1.33 \cdot 10^{-2}$	$3.33 \cdot 10^{-3}$
hexa <sub>2</sub>	40 301	80 604	$6.67 \cdot 10^{-3}$	$1.67 \cdot 10^{-3}$
hexa <sub>3</sub>	90 451	180 904	$4.44 \cdot 10^{-3}$	$1.11 \cdot 10^{-3}$
hexa <sub>4</sub>	160 601	321 204	$3.33 \cdot 10^{-3}$	$8.33 \cdot 10^{-4}$
hexa <sub>5</sub>	250 751	501 504	$2.67 \cdot 10^{-3}$	$6.67 \cdot 10^{-4}$
hexa <sub>6</sub>	360 901	721 804	$2.22 \cdot 10^{-3}$	$5.56 \cdot 10^{-4}$
hexa <sub>7</sub>	491 051	982 104	$1.90 \cdot 10^{-3}$	$4.76 \cdot 10^{-4}$
hexa <sub>8</sub>	641 201	1 282 404	$1.67 \cdot 10^{-3}$	$4.17 \cdot 10^{-4}$
hexa <sub>9</sub>	811 351	1 622 704	$1.48 \cdot 10^{-3}$	$3.70 \cdot 10^{-4}$
hexa <sub>10</sub>	1 001 501	2 003 004	$1.33 \cdot 10^{-3}$	$3.33 \cdot 10^{-4}$

TABLE 2. Condition number  $\kappa$  of matrix  $A$  with and without AMG preconditioning on the *hexagonal meshes* of Table 1.

Mesh	rtol	No Prec	c-GAMG	a-GAMG	BoomerAMG	ML
		$\kappa$	$\kappa$	$\kappa$	$\kappa$	$\kappa$ (its)
hexa <sub>1</sub>	4.51e-16	7.74e+02 (109)	1.12 (10)	1.52 (15)	1.31 (13)	1.66 (15)
hexa <sub>2</sub>	9.36e-16	3.09e+03 (141)	1.14 (10)	1.75 (16)	1.39 (14)	1.97 (18)
hexa <sub>3</sub>	1.38e-15	6.96e+03 (194)	1.18 (11)	1.69 (17)	1.49 (15)	2.22 (20)
hexa <sub>4</sub>	1.85e-15	1.24e+04 (255)	1.18 (11)	1.92 (18)	1.52 (15)	2.51 (22)
hexa <sub>5</sub>	2.38e-15	1.93e+04 (316)	1.20 (11)	1.95 (18)	1.56 (16)	2.91 (23)
hexa <sub>6</sub>	2.80e-15	2.78e+04 (377)	1.23 (12)	2.01 (19)	1.63 (16)	3.12 (24)
hexa <sub>7</sub>	3.28e-15	3.79e+04 (438)	1.24 (12)	2.13 (19)	1.61 (16)	3.37 (25)
hexa <sub>8</sub>	3.73e-15	4.95e+04 (492)	1.26 (12)	2.18 (20)	1.72 (17)	3.87 (26)
hexa <sub>9</sub>	4.25e-15	6.26e+04 (545)	1.27 (12)	2.14 (20)	1.72 (17)	3.94 (26)
hexa <sub>10</sub>	4.89e-15	7.73e+04 (595)	1.27 (12)	2.25 (20)	1.80 (17)	4.05 (27)

of snowflakes cells, it still exhibits a high number of iterations, thereby worsening its computational performance, as we will see in the next sections.

**4.1. Discontinuous coefficients.** We now want to test robustness of AMG preconditioners when discontinuous, highly heterogeneous coefficients  $\rho$  are considered. We build a “checkerboard” pattern

FIGURE 2. Example of Voronoi mesh.

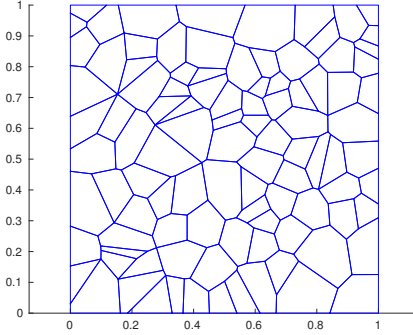


TABLE 3. Meshes of Voronoi cells used in the experiments.

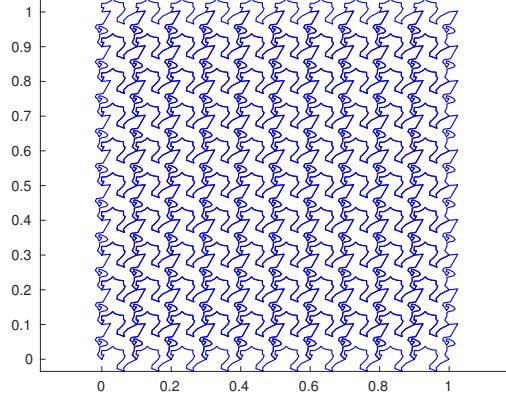
Mesh	$N_{\text{elt}}$	$N_v$	$h$	$h_{\min}$	$\gamma_0$	$\gamma_1$
vor <sub>01</sub>	2500	5006	$6.38 \cdot 10^{-2}$	$6.19 \cdot 10^{-6}$	$1.42 \cdot 10^1$	$5.85 \cdot 10^3$
vor <sub>02</sub>	5000	10 008	$4.34 \cdot 10^{-2}$	$5.85 \cdot 10^{-7}$	$1.46 \cdot 10^1$	$3.40 \cdot 10^4$
vor <sub>03</sub>	10 000	20 007	$3.47 \cdot 10^{-2}$	$1.73 \cdot 10^{-7}$	$2.53 \cdot 10^1$	$9.49 \cdot 10^4$
vor <sub>04</sub>	20 000	40 011	$2.41 \cdot 10^{-2}$	$2.14 \cdot 10^{-7}$	$2.09 \cdot 10^1$	$7.25 \cdot 10^4$
vor <sub>05</sub>	40 000	80 007	$1.73 \cdot 10^{-2}$	$8.26 \cdot 10^{-8}$	$2.68 \cdot 10^1$	$7.18 \cdot 10^4$
vor <sub>06</sub>	80 000	160 028	$1.14 \cdot 10^{-2}$	$6.00 \cdot 10^{-9}$	$2.88 \cdot 10^1$	$1.10 \cdot 10^6$
vor <sub>07</sub>	160 000	320 020	$8.86 \cdot 10^{-3}$	$4.02 \cdot 10^{-9}$	$3.14 \cdot 10^1$	$1.24 \cdot 10^6$
vor <sub>08</sub>	320 000	640 035	$6.25 \cdot 10^{-3}$	$3.59 \cdot 10^{-9}$	$3.07 \cdot 10^1$	$9.57 \cdot 10^5$
vor <sub>09</sub>	640 000	1 280 053	$4.36 \cdot 10^{-3}$	$1.14 \cdot 10^{-9}$	$4.04 \cdot 10^1$	$1.91 \cdot 10^6$
vor <sub>010</sub>	1 280 000	2 560 065	$3.39 \cdot 10^{-3}$	$7.50 \cdot 10^{-10}$	$5.08 \cdot 10^1$	$2.29 \cdot 10^6$

as follows: we deal with five of the hexagonal meshes in Table 1 (in particular, hexa<sub>2</sub>, hexa<sub>4</sub>, hexa<sub>6</sub>, hexa<sub>8</sub> and hexa<sub>10</sub>) and the eight finest meshes in Table 4 and partition their polygons into an increasing number of parts  $L$  ( $L = 64, 128, 256, 512$  and  $1024$ ) by using METIS [36]. Every element

TABLE 4. Condition number  $\kappa$  of matrix  $A$  with and without AMG preconditioning on the *Voronoi meshes* of Table 3. With mesh vor<sub>010</sub>, CG without preconditioning requires more than 10000 iterations to reach convergence.

Mesh	rtol	No Prec	c-GAMG	a-GAMG	BoomerAMG	ML
		$\kappa$	$\kappa$	$\kappa$	$\kappa$	$\kappa$
vor <sub>01</sub>	3.50e-14	2.79e+03 (371)	1.43 (12)	2.09 (17)	1.41 (13)	2.60 (19)
vor <sub>02</sub>	7.34e-14	6.91e+03 (553)	1.63 (12)	2.50 (19)	1.48 (13)	3.04 (22)
vor <sub>03</sub>	1.45e-13	1.55e+04 (827)	1.81 (14)	2.65 (20)	1.54 (13)	3.76 (24)
vor <sub>04</sub>	2.88e-13	3.44e+04 (1141)	1.90 (15)	3.12 (21)	1.55 (13)	4.29 (25)
vor <sub>05</sub>	5.83e-13	7.87e+04 (1736)	2.04 (15)	3.27 (21)	1.89 (14)	4.50 (27)
vor <sub>06</sub>	1.19e-12	1.36e+05 (2383)	2.41 (17)	3.53 (22)	1.80 (14)	5.56 (28)
vor <sub>07</sub>	2.41e-12	3.52e+05 (3633)	2.72 (18)	3.99 (23)	1.78 (14)	6.41 (30)
vor <sub>08</sub>	4.21e-12	8.98e+05 (5412)	3.32 (19)	4.23 (23)	2.03 (15)	8.20 (32)
vor <sub>09</sub>	9.70e-12	2.15e+06 (7775)	3.92 (20)	4.77 (24)	2.38 (15)	8.18 (33)
vor <sub>010</sub>	1.34e-11	-	4.11 (21)	5.24 (25)	2.22 (15)	10.00 (35)

FIGURE 3. Example of mesh of "horse" cells.

TABLE 5. Meshes of horse cells used in the experiments; for all of these meshes,  $\gamma_1 = 39$ .

Mesh	$N_{\text{elt}}$	$N_v$	$h$	$h_{\min}$
horse <sub>1</sub>	2500	94 401	$3.52 \cdot 10^{-2}$	$9.01 \cdot 10^{-4}$
horse <sub>2</sub>	3600	135 481	$2.93 \cdot 10^{-2}$	$7.51 \cdot 10^{-4}$
horse <sub>3</sub>	4900	183 961	$2.51 \cdot 10^{-2}$	$6.44 \cdot 10^{-4}$
horse <sub>4</sub>	6400	239 841	$2.20 \cdot 10^{-2}$	$5.63 \cdot 10^{-4}$
horse <sub>5</sub>	8100	303 121	$1.95 \cdot 10^{-2}$	$5.01 \cdot 10^{-4}$
horse <sub>6</sub>	10 000	373 801	$1.76 \cdot 10^{-2}$	$4.51 \cdot 10^{-4}$
horse <sub>7</sub>	12 100	451 881	$1.60 \cdot 10^{-2}$	$4.10 \cdot 10^{-4}$
horse <sub>8</sub>	14 400	537 361	$1.46 \cdot 10^{-2}$	$3.76 \cdot 10^{-4}$
horse <sub>9</sub>	16 900	630 241	$1.35 \cdot 10^{-2}$	$3.47 \cdot 10^{-4}$
horse <sub>10</sub>	19 600	730 521	$1.26 \cdot 10^{-2}$	$3.22 \cdot 10^{-4}$

TABLE 6. Condition number  $\kappa$  of matrix  $A$  with and without AMG preconditioning on meshes of *horses* (see Table 5).

Mesh	rtol	No Prec	c-GAMG	a-GAMG	BoomerAMG	ML
		$\kappa$	$\kappa$	$\kappa$	$\kappa$	$\kappa$
horse <sub>1</sub>	1.15e-13	8.82e+04 (2071)	127.55 (111)	19.84 (59)	3.42 (24)	30.00 (72)
horse <sub>2</sub>	1.53e-13	1.28e+05 (2467)	183.06 (130)	20.63 (60)	3.61 (24)	30.43 (73)
horse <sub>3</sub>	1.95e-13	1.75e+05 (2837)	243.36 (151)	22.14 (62)	3.49 (24)	32.66 (76)
horse <sub>4</sub>	2.37e-13	2.29e+05 (3204)	349.99 (176)	22.87 (64)	3.82 (25)	36.46 (79)
horse <sub>5</sub>	2.83e-13	2.90e+05 (3583)	535.99 (206)	24.44 (66)	3.65 (25)	38.29 (81)
horse <sub>6</sub>	3.35e-13	3.60e+05 (3953)	485.97 (212)	25.30 (67)	3.81 (25)	41.80 (83)
horse <sub>7</sub>	3.85e-13	4.36e+05 (4273)	641.35 (232)	25.57 (67)	4.03 (25)	41.53 (84)
horse <sub>8</sub>	4.41e-13	5.19e+05 (4644)	741.34 (261)	26.23 (68)	4.05 (25)	39.89 (85)
horse <sub>9</sub>	4.98e-13	6.10e+05 (5007)	894.57 (280)	27.14 (69)	4.00 (25)	41.65 (84)
horse <sub>10</sub>	5.57e-13	7.08e+05 (5375)	1009.26 (298)	27.59 (69)	4.11 (25)	46.51 (89)

FIGURE 4. Mesh obtained by embedding the third iterate of the snowflake into rectangles.

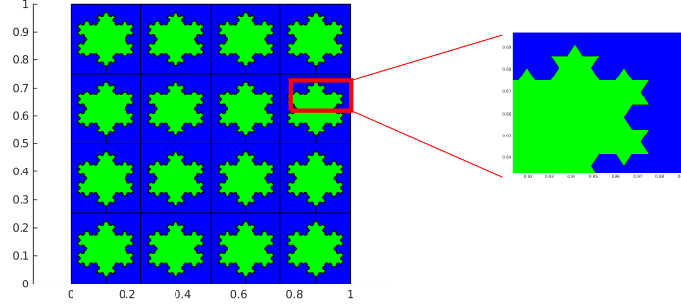


TABLE 7. Meshes with snowflakes cells. For all of these meshes,  $\gamma_1 \approx 68.55$ .

Mesh	$N_{\text{elt}}$	$N_v$	$h$	$h_{\min}$
koch <sub>1</sub>	288	27 973	$1.18 \cdot 10^{-1}$	$1.72 \cdot 10^{-3}$
koch <sub>2</sub>	512	49 713	$8.84 \cdot 10^{-2}$	$1.29 \cdot 10^{-3}$
koch <sub>3</sub>	800	77 661	$7.07 \cdot 10^{-2}$	$1.03 \cdot 10^{-3}$
koch <sub>4</sub>	1152	111 817	$5.89 \cdot 10^{-2}$	$8.60 \cdot 10^{-4}$
koch <sub>5</sub>	1568	152 181	$5.05 \cdot 10^{-2}$	$7.37 \cdot 10^{-4}$
koch <sub>6</sub>	2048	198 753	$4.42 \cdot 10^{-2}$	$6.45 \cdot 10^{-4}$
koch <sub>7</sub>	2592	251 533	$3.93 \cdot 10^{-2}$	$5.73 \cdot 10^{-4}$
koch <sub>8</sub>	3200	310 521	$3.54 \cdot 10^{-2}$	$5.16 \cdot 10^{-4}$
koch <sub>9</sub>	3872	375 717	$3.21 \cdot 10^{-2}$	$4.69 \cdot 10^{-4}$
koch <sub>10</sub>	4608	447 121	$2.95 \cdot 10^{-2}$	$4.30 \cdot 10^{-4}$
koch <sub>11</sub>	5408	524 733	$2.72 \cdot 10^{-2}$	$3.97 \cdot 10^{-4}$
koch <sub>12</sub>	6272	608 553	$2.53 \cdot 10^{-2}$	$3.68 \cdot 10^{-4}$
koch <sub>13</sub>	7200	698 581	$2.36 \cdot 10^{-2}$	$3.44 \cdot 10^{-4}$

TABLE 8. Condition number  $\kappa$  of matrix  $A$  on meshes with *snowflakes*.

Mesh	rtol	No Prec	c-GAMG	a-GAMG	BoomerAMG	ML
		$\kappa$	$\kappa$	$\kappa$	$\kappa$	$\kappa$
koch <sub>1</sub>	3.87e-13	8.41e+04 (1069)	46.51 (50)	15.49 (50)	64.08 (91)	8.76 (35)
koch <sub>2</sub>	7.38e-13	1.51e+05 (1430)	79.63 (63)	16.47 (53)	68.38 (91)	9.15 (35)
koch <sub>3</sub>	1.21e-12	2.37e+05 (1772)	126.33 (77)	17.38 (54)	71.51 (94)	10.40 (35)
koch <sub>4</sub>	1.74e-12	3.42e+05 (2117)	181.52 (89)	18.25 (55)	73.83 (94)	12.98 (35)
koch <sub>5</sub>	2.43e-12	4.67e+05 (2464)	251.53 (102)	20.44 (56)	75.60 (93)	13.80 (35)
koch <sub>6</sub>	3.19e-12	6.10e+05 (2632)	302.75 (110)	19.16 (55)	76.98 (92)	15.73 (35)
koch <sub>7</sub>	4.01e-12	7.73e+05 (2930)	414.78 (127)	19.64 (55)	77.81 (93)	15.87 (35)
koch <sub>8</sub>	4.96e-12	9.55e+05 (3182)	507.17 (138)	20.36 (56)	79.03 (93)	16.05 (35)
koch <sub>9</sub>	6.07e-12	1.16e+06 (3469)	629.20 (152)	20.06 (54)	79.80 (92)	17.63 (35)
koch <sub>10</sub>	7.38e-12	1.38e+06 (3670)	724.47 (158)	19.32 (54)	77.60 (91)	18.58 (35)
koch <sub>11</sub>	8.66e-12	1.61e+06 (3915)	867.05 (170)	19.76 (54)	81.06 (91)	19.66 (35)
koch <sub>12</sub>	9.74e-12	1.87e+06 (4141)	1018.24 (182)	20.40 (54)	81.51 (91)	19.89 (35)
koch <sub>13</sub>	1.14e-11	2.15e+06 (4384)	1101.59 (187)	19.97 (54)	80.98 (91)	20.52 (35)

in a given part is then assigned the same diffusion coefficient  $\rho = 10^\alpha$ , with  $\alpha$  random integer in  $[-5, 5]$ . The loading term is random uniform in  $[-1, 1]$ .

FIGURE 5. Mesh obtained by aggregating Voronoi cells. Boundaries of aggregates are marked in red.

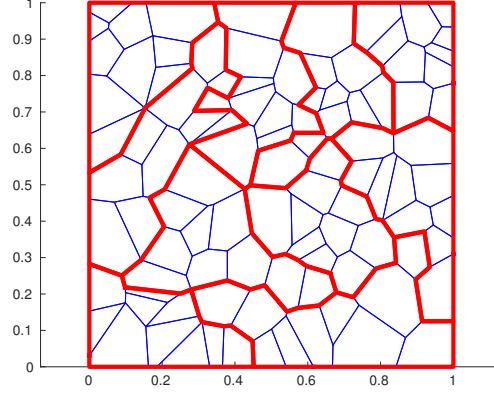


TABLE 9. Meshes of aggregates of Voronoi cells used in the experiments.

Mesh	$N_{\text{elt}}$	$N_v$	$h$	$h_{\min}$	$\gamma_1$
a-voro <sub>1</sub>	512	5652	$1.26 \cdot 10^{-1}$	$7.97 \cdot 10^{-7}$	$9.73 \cdot 10^4$
a-voro <sub>2</sub>	1024	11 190	$9.86 \cdot 10^{-2}$	$1.73 \cdot 10^{-7}$	$3.05 \cdot 10^5$
a-voro <sub>3</sub>	2048	22 250	$6.31 \cdot 10^{-2}$	$3.47 \cdot 10^{-7}$	$1.15 \cdot 10^5$
a-voro <sub>4</sub>	4096	44 615	$4.80 \cdot 10^{-2}$	$8.26 \cdot 10^{-8}$	$3.31 \cdot 10^5$
a-voro <sub>5</sub>	8192	89 283	$3.77 \cdot 10^{-2}$	$2.44 \cdot 10^{-8}$	$5.74 \cdot 10^5$
a-voro <sub>6</sub>	16 384	180 219	$2.78 \cdot 10^{-2}$	$4.02 \cdot 10^{-9}$	$4.39 \cdot 10^6$
a-voro <sub>7</sub>	32 768	365 921	$1.88 \cdot 10^{-2}$	$3.59 \cdot 10^{-9}$	$2.35 \cdot 10^6$
a-voro <sub>8</sub>	65 536	731 552	$1.40 \cdot 10^{-2}$	$1.14 \cdot 10^{-9}$	$6.98 \cdot 10^6$
a-voro <sub>9</sub>	131 072	1 471 656	$1.02 \cdot 10^{-2}$	$3.43 \cdot 10^{-9}$	$1.41 \cdot 10^6$

TABLE 10. *Aggregates of Voronoi cells* (Table 9). Condition number  $\kappa$  of matrix  $A$  with and without AMG preconditioning.

Mesh	rtol	No Prec	c-GAMG	a-GAMG	BoomerAMG	ML
		$\kappa$	$\kappa$	$\kappa$	$\kappa$	$\kappa$
a-voro <sub>1</sub>	4.20e-14	2.89e+03 (380)	3.45 (19)	4.00 (24)	1.92 (16)	5.37 (29)
a-voro <sub>2</sub>	8.10e-14	1.06e+04 (586)	5.68 (25)	6.01 (30)	2.09 (17)	8.34 (35)
a-voro <sub>3</sub>	1.60e-13	1.62e+04 (833)	8.87 (31)	6.73 (32)	1.90 (16)	8.62 (37)
a-voro <sub>4</sub>	3.24e-13	3.84e+04 (1258)	14.49 (41)	7.67 (35)	2.06 (16)	10.33 (41)
a-voro <sub>5</sub>	6.67e-13	1.04e+05 (1817)	28.81 (55)	10.28 (40)	2.51 (17)	14.89 (47)
a-voro <sub>6</sub>	1.37e-12	2.03e+05 (2710)	79.60 (77)	10.96 (41)	4.14 (19)	17.58 (49)
a-voro <sub>7</sub>	2.81e-12	4.12e+05 (3994)	141.87 (114)	12.42 (42)	2.62 (18)	19.46 (52)
a-voro <sub>8</sub>	5.70e-12	9.36e+05 (5690)	247.73 (154)	13.56 (44)	2.85 (18)	23.09 (56)
a-voro <sub>9</sub>	8.55e-13	2.05e+06 (8410)	515.85 (229)	14.94 (49)	3.22 (20)	24.07 (63)

Here, convergence is decided by the *absolute* size of the residual norm `abstol` obtained with the direct solver SuperLU\_DIST (see Tables 13, 14). Results are displayed in Table 15 and Figure 7 for hexagonal meshes, and in Table 16 and Figure 8 for Voronoi meshes. We point out that, with highly oscillating coefficients, CG without AMG preconditioning does not attain convergence on any mesh.

FIGURE 6. Mesh obtained by aggregating horse cells. Boundaries of aggregates are marked in red.

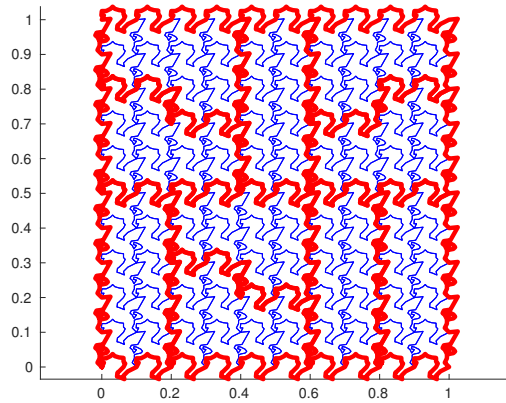


TABLE 11. Meshes of aggregated horse cells used in the experiments.

Mesh	$N_{\text{elt}}$	$N_v$	$h$	$h_{\min}$	$\gamma_1$
a-horse <sub>1</sub>	250	42 621	$1.61 \cdot 10^{-1}$	$9.01 \cdot 10^{-4}$	$1.79 \cdot 10^2$
a-horse <sub>2</sub>	360	61 151	$1.47 \cdot 10^{-1}$	$7.51 \cdot 10^{-4}$	$1.96 \cdot 10^2$
a-horse <sub>3</sub>	490	82 007	$1.25 \cdot 10^{-1}$	$6.44 \cdot 10^{-4}$	$1.94 \cdot 10^2$
a-horse <sub>4</sub>	640	107 899	$1.08 \cdot 10^{-1}$	$5.63 \cdot 10^{-4}$	$1.92 \cdot 10^2$
a-horse <sub>5</sub>	810	134 589	$1.00 \cdot 10^{-1}$	$5.01 \cdot 10^{-4}$	$2.00 \cdot 10^2$
a-horse <sub>6</sub>	1000	168 525	$9.03 \cdot 10^{-2}$	$4.51 \cdot 10^{-4}$	$2.00 \cdot 10^2$

TABLE 12. Condition number  $\kappa$  of matrix  $A$  with and without AMG preconditioning on meshes of *aggregated horses*. ML fails on all the meshes due to an internal *Segment Violation* error.

Mesh	rtol	No Prec	c-GAMG	a-GAMG	BoomerAMG	ML
		$\kappa$	$\kappa$	$\kappa$	$\kappa$	$\kappa$
a-horse <sub>1</sub>	8.31e-14	1.44e+05 (1896)	182.00 (82)	51.36 (73)	22.66 (60)	-
a-horse <sub>2</sub>	1.28e-13	2.58e+05 (2625)	267.76 (106)	61.17 (87)	40.17 (69)	-
a-horse <sub>3</sub>	1.81e-13	3.37e+05 (3221)	355.49 (125)	67.09 (97)	41.09 (69)	-
a-horse <sub>4</sub>	1.95e-13	4.61e+05 (3874)	473.41 (151)	78.85 (108)	25.67 (69)	-
a-horse <sub>5</sub>	2.71e-13	6.47e+05 (4456)	643.31 (171)	82.15 (115)	34.73 (67)	-
a-horse <sub>6</sub>	2.83e-13	8.11e+05 (5099)	728.71 (189)	96.54 (120)	39.74 (75)	-

Tables 15 and 16 show that only BoomerAMG, for both hexagonal and Voronoi meshes, is performing well even with highly oscillating coefficients; the iteration count of BoomerAMG does not depend on the size of the jump of the diffusion coefficient and on the problem size, see Figures 7-8 where we used a logarithmic scale for the x-axis.

**4.2. Performance Comparison of Direct and Iterative Solvers.** Finally we compare the performance of several direct and iterative solvers available in PETSCs by measuring the elapsed time for both setup and solving. We recall that, for iterative methods, convergence was decided by the

TABLE 13. Absolute size of the residual norm `abstol` obtained with the direct solver SuperLU\_DIST on the hexagonal meshes partitioned with METIS with random data.

Mesh\ $\backslash$ $L$	64	128	256	512	1024
hexa <sub>2</sub>	$3.38 \cdot 10^{-15}$	$2.75 \cdot 10^{-12}$	$1.66 \cdot 10^{-13}$	$6.29 \cdot 10^{-13}$	$1.10 \cdot 10^{-12}$
hexa <sub>4</sub>	$4.66 \cdot 10^{-15}$	$3.93 \cdot 10^{-14}$	$3.01 \cdot 10^{-13}$	$1.40 \cdot 10^{-13}$	$1.72 \cdot 10^{-13}$
hexa <sub>6</sub>	$7.40 \cdot 10^{-16}$	$6.40 \cdot 10^{-15}$	$3.23 \cdot 10^{-13}$	$9.88 \cdot 10^{-13}$	$1.65 \cdot 10^{-12}$
hexa <sub>8</sub>	$1.15 \cdot 10^{-15}$	$7.97 \cdot 10^{-13}$	$4.44 \cdot 10^{-13}$	$4.14 \cdot 10^{-13}$	$1.16 \cdot 10^{-13}$
hexa <sub>10</sub>	$2.30 \cdot 10^{-15}$	$1.38 \cdot 10^{-12}$	$1.47 \cdot 10^{-13}$	$1.33 \cdot 10^{-13}$	$4.10 \cdot 10^{-12}$

TABLE 14. Absolute size of the residual norm `abstol` obtained with the direct solver SuperLU\_DIST on the Voronoi meshes partitioned with METIS with random data.

Mesh\ $\backslash$ $L$	64	128	256	512	1024
vor <sub>3</sub>	$3.64 \cdot 10^{-16}$	$3.27 \cdot 10^{-12}$	$4.94 \cdot 10^{-13}$	$1.26 \cdot 10^{-12}$	$2.15 \cdot 10^{-13}$
vor <sub>4</sub>	$4.64 \cdot 10^{-15}$	$4.04 \cdot 10^{-14}$	$2.19 \cdot 10^{-14}$	$8.52 \cdot 10^{-14}$	$3.84 \cdot 10^{-13}$
vor <sub>5</sub>	$1.12 \cdot 10^{-14}$	$6.37 \cdot 10^{-13}$	$4.92 \cdot 10^{-13}$	$5.05 \cdot 10^{-13}$	$2.67 \cdot 10^{-13}$
vor <sub>6</sub>	$5.36 \cdot 10^{-15}$	$1.15 \cdot 10^{-12}$	$1.68 \cdot 10^{-13}$	$3.39 \cdot 10^{-12}$	$5.32 \cdot 10^{-13}$
vor <sub>7</sub>	$7.15 \cdot 10^{-16}$	$4.62 \cdot 10^{-13}$	$3.05 \cdot 10^{-13}$	$1.47 \cdot 10^{-13}$	$1.44 \cdot 10^{-12}$
vor <sub>8</sub>	$1.29 \cdot 10^{-14}$	$3.82 \cdot 10^{-14}$	$5.99 \cdot 10^{-14}$	$1.58 \cdot 10^{-13}$	$1.53 \cdot 10^{-12}$
vor <sub>9</sub>	$9.56 \cdot 10^{-16}$	$1.15 \cdot 10^{-12}$	$3.47 \cdot 10^{-13}$	$1.83 \cdot 10^{-12}$	$3.80 \cdot 10^{-13}$
vor <sub>10</sub>	$2.58 \cdot 10^{-15}$	$3.42 \cdot 10^{-14}$	$3.01 \cdot 10^{-13}$	$3.14 \cdot 10^{-13}$	$1.44 \cdot 10^{-13}$

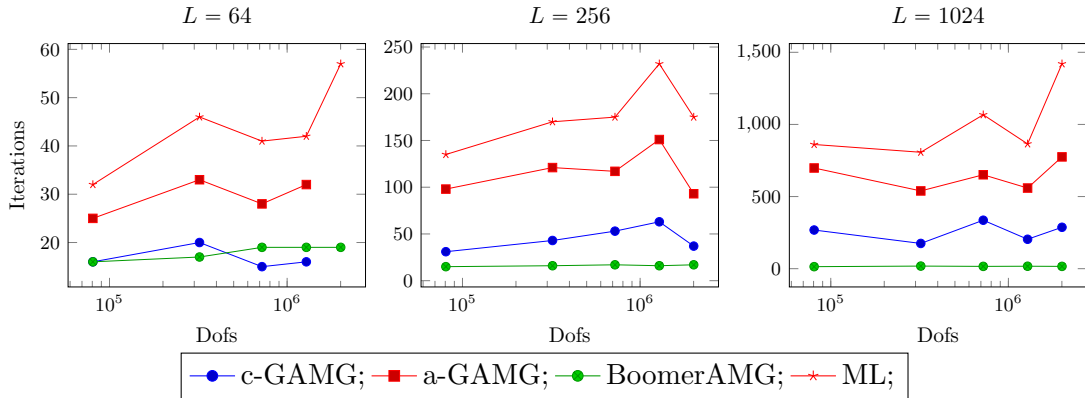


FIGURE 7. Discontinuous coefficients  $\rho$ . Number of iterations of PCG with different AMG preconditioners in a logarithmic scale for the x-axis and for the hexagonal meshes hexa<sub>2</sub>, hexa<sub>4</sub>, hexa<sub>6</sub>, hexa<sub>8</sub> and hexa<sub>10</sub> of Table 1 partitioned in  $L = 64, 256, 1024$  parts.

decrease of either the relative or the absolute residual norm as obtained with the direct solver SuperLU\_DIST (see `rtol` and `abstol` reported in each Table). Figures 9,10, 11, 12 and 13 display the time in seconds (for setup and solving) for both direct and direct solvers in a loglog scale.

The best results are obtained with BoomerAMG and/or with ML for hexagonal, Voronoi and horse meshes, as well as for meshes of aggregated Voronoi cells. Conversely, when considering Koch snowflake meshes and aggregates of horse cells, direct methods outperform AMG preconditioners.

TABLE 15. Discontinuous coefficients  $\rho$ . Condition number  $\kappa$  of matrix  $A$  with AMG preconditioning on the hexagonal meshes  $\text{hexa}_2$ ,  $\text{hexa}_4$ ,  $\text{hexa}_6$ ,  $\text{hexa}_8$  and  $\text{hexa}_{10}$  of Table 1 partitioned in  $L$  parts.

c-GAMG					
Mesh\ $L$	64	128	256	512	1024
$\text{hexa}_2$	$2.30 \cdot 10^1$	$2.43 \cdot 10^3$	$1.25 \cdot 10^2$	$2.25 \cdot 10^3$	$6.38 \cdot 10^3$
$\text{hexa}_4$	$6.48 \cdot 10^1$	$2.11 \cdot 10^2$	$4.08 \cdot 10^3$	$1.60 \cdot 10^3$	$1.72 \cdot 10^4$
$\text{hexa}_6$	1.85	$6.69 \cdot 10^1$	$1.87 \cdot 10^4$	$6.04 \cdot 10^3$	$4.73 \cdot 10^4$
$\text{hexa}_8$	4.73	-	$4.95 \cdot 10^3$	$3.07 \cdot 10^4$	$2.10 \cdot 10^4$
$\text{hexa}_{10}$	-	$1.36 \cdot 10^3$	$9.64 \cdot 10^2$	$2.22 \cdot 10^3$	$8.51 \cdot 10^4$
a-GAMG					
Mesh\ $L$	64	128	256	512	1024
$\text{hexa}_2$	$2.16 \cdot 10^1$	$3.25 \cdot 10^5$	$1.21 \cdot 10^4$	$2.75 \cdot 10^5$	$1.23 \cdot 10^6$
$\text{hexa}_4$	$6.94 \cdot 10^2$	$8.06 \cdot 10^2$	$1.11 \cdot 10^4$	$6.57 \cdot 10^3$	$5.09 \cdot 10^4$
$\text{hexa}_6$	$2.21 \cdot 10^1$	$2.28 \cdot 10^2$	$1.00 \cdot 10^4$	$4.96 \cdot 10^4$	$5.06 \cdot 10^5$
$\text{hexa}_8$	$1.59 \cdot 10^2$	-	$4.06 \cdot 10^4$	$2.07 \cdot 10^5$	$4.21 \cdot 10^4$
$\text{hexa}_{10}$	-	$1.01 \cdot 10^5$	$2.99 \cdot 10^3$	$2.99 \cdot 10^4$	$3.96 \cdot 10^5$
BoomerAMG					
Mesh\ $L$	64	128	256	512	1024
$\text{hexa}_2$	1.68	1.97	1.78	2.12	1.85
$\text{hexa}_4$	1.90	1.79	1.80	1.88	2.56
$\text{hexa}_6$	2.69	2.02	2.04	2.52	2.14
$\text{hexa}_8$	2.01	2.03	1.96	2.36	2.08
$\text{hexa}_{10}$	1.90	2.07	2.06	2.16	2.66
ML					
Mesh\ $L$	64	128	256	512	1024
$\text{hexa}_2$	$2.85 \cdot 10^2$	$1.32 \cdot 10^6$	$1.22 \cdot 10^4$	$4.02 \cdot 10^5$	$7.81 \cdot 10^5$
$\text{hexa}_4$	$1.56 \cdot 10^3$	$3.60 \cdot 10^3$	$2.63 \cdot 10^4$	$1.70 \cdot 10^5$	$7.01 \cdot 10^4$
$\text{hexa}_6$	$1.14 \cdot 10^2$	$1.03 \cdot 10^3$	$9.52 \cdot 10^3$	$1.67 \cdot 10^5$	$1.21 \cdot 10^6$
$\text{hexa}_8$	$1.07 \cdot 10^3$	$1.13 \cdot 10^5$	$1.12 \cdot 10^5$	$1.69 \cdot 10^6$	$6.88 \cdot 10^5$
$\text{hexa}_{10}$	$2.11 \cdot 10^2$	$4.81 \cdot 10^5$	$1.02 \cdot 10^4$	$7.78 \cdot 10^5$	$6.84 \cdot 10^5$

We recall that AMG preconditioners require a high number of iterations for these meshes, as shown in Figure 10-right and 11-right and Tables 8, 12, thereby worsening their performance.

Clearly, a more accurate evaluation of the efficiency of AMG techniques for this type of meshes would require a deeper analysis (outside the scope of this work), such as an ad-hoc tuning of the AMG parameters or a more accurate analysis of the matrices involved.

## 5. CONCLUSION

We numerically investigated the performance of AMG preconditioners for the solution of a model elliptic problem on polygonal meshes employing the virtual element method. The tested meshes range from the most regular hexagonal to more complex and challenging grids that may mimic features of more realistic problems such as those based on periodic cellular structures. Our results show that CG accelerated multigrid (AMG/CG) is very effective when dealing with either regular (hexagonal) or Voronoi and aggregates of Voronoi meshes. Moreover, our tests showed that BoomerAMG is also

TABLE 16. Discontinuous coefficients  $\rho$ . Condition number  $\kappa$  of matrix  $A$  with AMG preconditioning on the Voronoi meshes  $\text{voro}_3$ – $\text{voro}_{10}$  of Table 4 partitioned in  $L$  parts.

c-GAMG					
Mesh\ $\backslash$ $L$	64	128	256	512	1024
$\text{voro}_3$	$1.95 \cdot 10^1$	$4.81 \cdot 10^5$	$8.47 \cdot 10^3$	$1.63 \cdot 10^5$	$6.12 \cdot 10^5$
$\text{voro}_4$	$2.99 \cdot 10^2$	$7.45 \cdot 10^2$	$1.97 \cdot 10^3$	$2.16 \cdot 10^4$	$5.14 \cdot 10^4$
$\text{voro}_5$	$4.54 \cdot 10^2$	$8.71 \cdot 10^3$	$1.73 \cdot 10^4$	$2.95 \cdot 10^5$	$1.17 \cdot 10^5$
$\text{voro}_6$	$6.25 \cdot 10^1$	$2.29 \cdot 10^4$	$2.09 \cdot 10^4$	$6.28 \cdot 10^3$	$3.07 \cdot 10^5$
$\text{voro}_7$	$3.66 \cdot 10^1$	$1.02 \cdot 10^6$	$2.12 \cdot 10^4$	$2.43 \cdot 10^5$	$8.01 \cdot 10^5$
$\text{voro}_8$	$1.10 \cdot 10^2$	$7.89 \cdot 10^3$	$3.00 \cdot 10^4$	$8.59 \cdot 10^4$	$4.31 \cdot 10^5$
$\text{voro}_9$	$7.71 \cdot 10^1$	$2.84 \cdot 10^5$	$1.86 \cdot 10^4$	$3.19 \cdot 10^5$	$2.60 \cdot 10^5$
$\text{voro}_{10}$	$8.50 \cdot 10^2$	$1.40 \cdot 10^4$	$1.14 \cdot 10^5$	$9.28 \cdot 10^4$	$6.33 \cdot 10^5$
a-GAMG					
Mesh\ $\backslash$ $L$	64	128	256	512	1024
$\text{voro}_3$	$2.15 \cdot 10^1$	$8.81 \cdot 10^5$	$3.45 \cdot 10^4$	$1.78 \cdot 10^5$	$5.60 \cdot 10^5$
$\text{voro}_4$	$1.79 \cdot 10^2$	$4.59 \cdot 10^2$	$3.93 \cdot 10^3$	$3.46 \cdot 10^4$	$8.90 \cdot 10^5$
$\text{voro}_5$	$2.28 \cdot 10^1$	$1.42 \cdot 10^4$	$1.24 \cdot 10^4$	$3.24 \cdot 10^5$	$4.04 \cdot 10^5$
$\text{voro}_6$	$1.19 \cdot 10^3$	$3.21 \cdot 10^4$	$1.90 \cdot 10^4$	$4.76 \cdot 10^5$	$1.19 \cdot 10^5$
$\text{voro}_7$	$4.38 \cdot 10^1$	$4.34 \cdot 10^5$	$2.04 \cdot 10^4$	$5.07 \cdot 10^4$	$2.85 \cdot 10^5$
$\text{voro}_8$	$1.37 \cdot 10^3$	$3.73 \cdot 10^3$	$1.95 \cdot 10^4$	$4.22 \cdot 10^4$	$7.12 \cdot 10^5$
$\text{voro}_9$	$9.64 \cdot 10^1$	$1.96 \cdot 10^4$	$2.69 \cdot 10^4$	$1.47 \cdot 10^6$	$2.02 \cdot 10^5$
$\text{voro}_{10}$	$6.93 \cdot 10^1$	$5.75 \cdot 10^3$	$1.39 \cdot 10^5$	$1.48 \cdot 10^5$	$6.78 \cdot 10^4$
BoomerAMG					
Mesh\ $\backslash$ $L$	64	128	256	512	1024
$\text{voro}_3$	1.95	1.86	1.87	2.08	2.25
$\text{voro}_4$	2.60	2.00	2.32	2.25	4.43
$\text{voro}_5$	2.19	2.17	2.31	2.11	2.16
$\text{voro}_6$	2.03	2.33	2.02	2.26	2.07
$\text{voro}_7$	2.06	2.50	2.48	3.03	3.16
$\text{voro}_8$	2.13	4.14	2.15	3.19	3.25
$\text{voro}_9$	2.38	2.41	2.36	2.57	2.75
$\text{voro}_{10}$	2.87	2.35	3.85	2.82	3.01
ML					
Mesh\ $\backslash$ $L$	64	128	256	512	1024
$\text{voro}_3$	$1.13 \cdot 10^2$	$1.32 \cdot 10^6$	$8.30 \cdot 10^4$	$2.66 \cdot 10^5$	$4.68 \cdot 10^5$
$\text{voro}_4$	$6.51 \cdot 10^2$	$3.70 \cdot 10^3$	$9.43 \cdot 10^3$	$4.15 \cdot 10^5$	$9.91 \cdot 10^6$
$\text{voro}_5$	$2.11 \cdot 10^3$	$1.79 \cdot 10^4$	$7.14 \cdot 10^4$	$5.12 \cdot 10^5$	$7.01 \cdot 10^5$
$\text{voro}_6$	$3.32 \cdot 10^1$	$2.97 \cdot 10^5$	$9.32 \cdot 10^4$	$3.20 \cdot 10^6$	$7.28 \cdot 10^5$
$\text{voro}_7$	$4.31 \cdot 10^2$	$2.11 \cdot 10^6$	$1.44 \cdot 10^5$	$2.15 \cdot 10^5$	$1.79 \cdot 10^6$
$\text{voro}_8$	$1.94 \cdot 10^4$	$3.85 \cdot 10^4$	$4.74 \cdot 10^4$	$9.44 \cdot 10^4$	$6.93 \cdot 10^5$
$\text{voro}_9$	$3.39 \cdot 10^2$	$6.85 \cdot 10^4$	$1.12 \cdot 10^5$	$1.96 \cdot 10^6$	$9.19 \cdot 10^5$
$\text{voro}_{10}$	$1.47 \cdot 10^3$	$2.00 \cdot 10^4$	$3.36 \cdot 10^5$	$5.14 \cdot 10^5$	$1.54 \cdot 10^5$

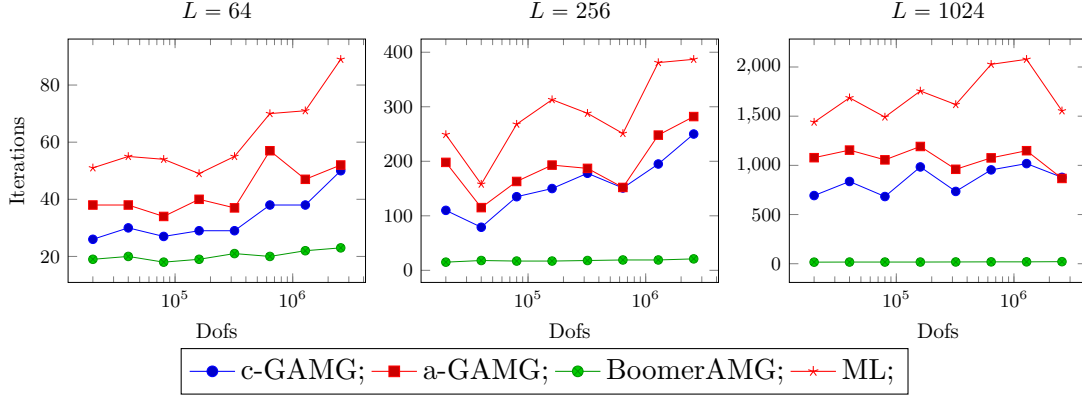


FIGURE 8. Discontinuous coefficients  $\rho$ . Number of iterations of PCG with different AMG preconditioners in a logarithmic scale for the x-axis and for the Voronoi meshes  $\text{vor}_{03}$ – $\text{vor}_{10}$  of Table 4 partitioned in  $L = 64, 256, 1024$  parts.

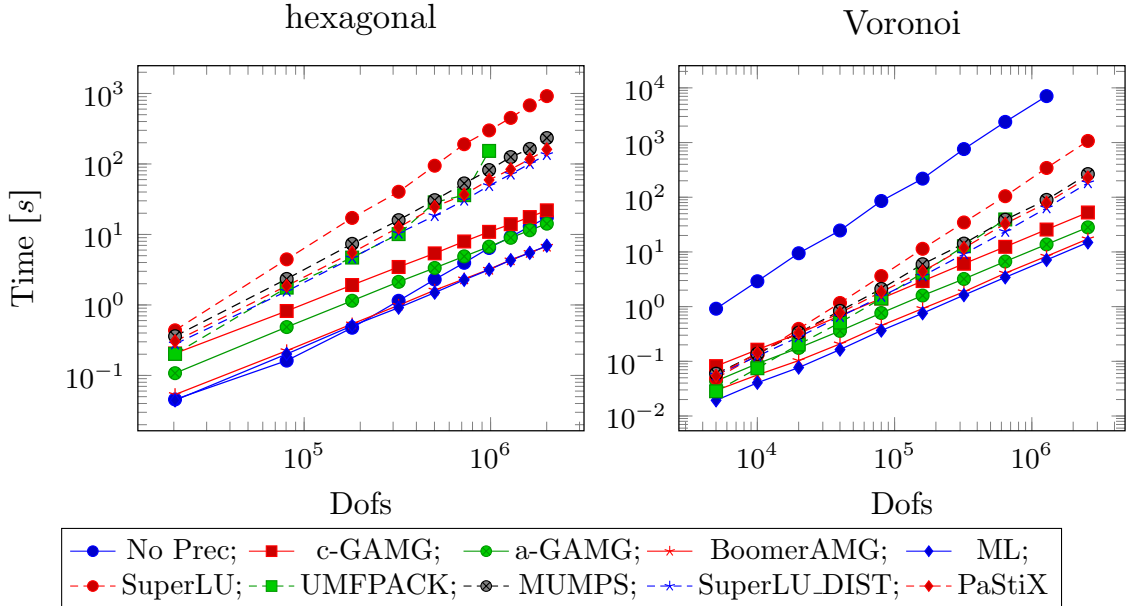


FIGURE 9. Time (for setup and solving) of direct and iterative solvers in a loglog scale for the *hexagonal meshes* of Table 1 and for the *Voronoi meshes* of Table 3. With mesh  $\text{vor}_{10}$ , CG without preconditioning requires more than 10000 iterations to reach convergence. With meshes  $\text{vor}_9$ ,  $\text{vor}_{10}$  and  $\text{hexa}_8$ ,  $\text{hexa}_9$ ,  $\text{hexa}_{10}$  UMFPACK fails due to an *out of memory* error.

robust if highly varying diffusion coefficients are considered for both set of meshes considered. Hinging on the results of the present paper, the adoption of AMG preconditioners (in particular BoomerAMG) seems to be a promising approach for solving large linear systems of equations associated with a VEM discretization, in terms of both scalability and reduction of the overall computational cost.

However, we also verified that, when more complex and challenging meshes are taken into account, such as meshes with many tiny (when compared to the diameter of the elements) edges, most of the considered AMG preconditioners do not preserve scalability, whilst those that retain it, like BoomerAMG or ML, lose most of their efficiency. Certainly, the linear system associated with the

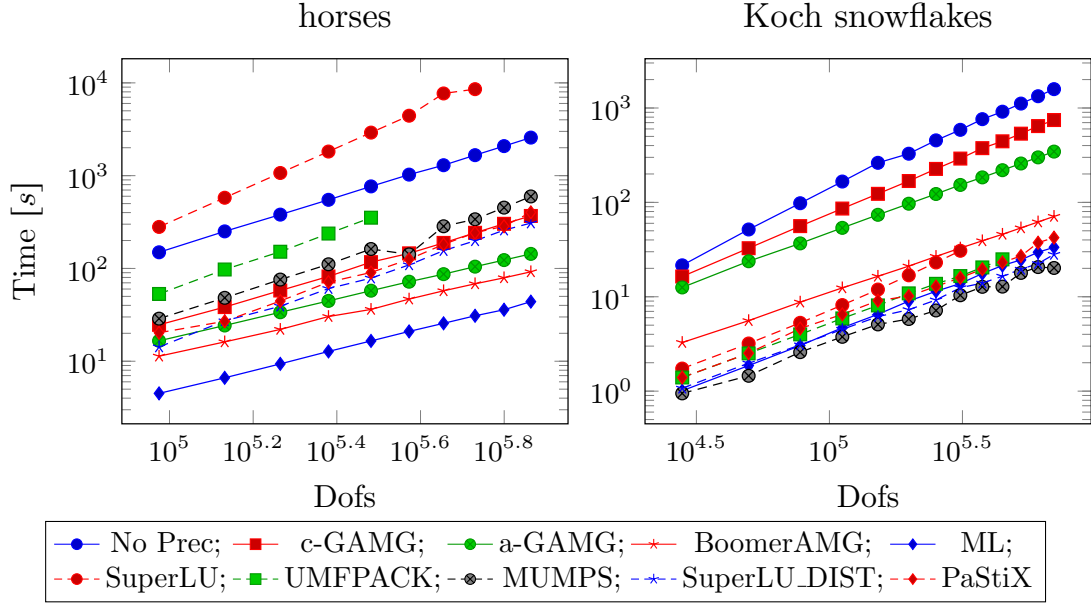


FIGURE 10. Time (for setup and solving) of direct and iterative solvers in a loglog scale for *meshes of horses* (Table 5) and for meshes with *Koch snowflakes* (Table 7). SuperLU fails due to an *out of memory* error on meshes horse<sub>9</sub> and horse<sub>10</sub> and koch<sub>9</sub>–koch<sub>13</sub> whereas UMFPACK fails on meshes horse<sub>6</sub>–horse<sub>10</sub> and koch<sub>11</sub>–koch<sub>13</sub>.

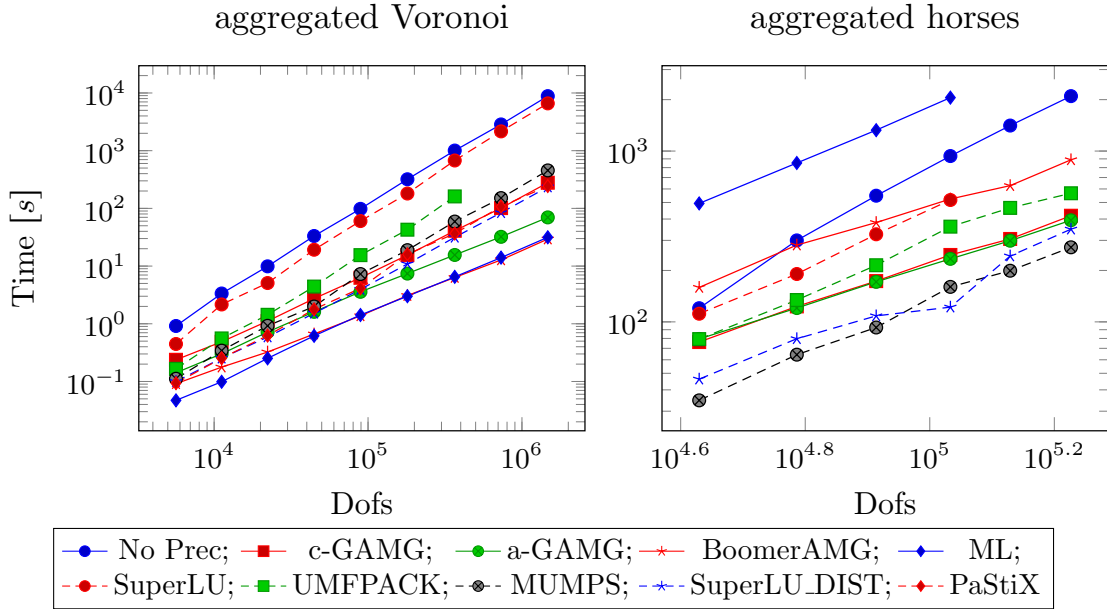


FIGURE 11. Time (for setup and solving) of direct and iterative solvers in a loglog scale for meshes of *aggregated Voronoi* and *aggregated horses* (Tables 9-11). Both SuperLU and UMFPACK fails on a-horse<sub>5</sub> and a-horse<sub>6</sub> due to an *out of memory* error.

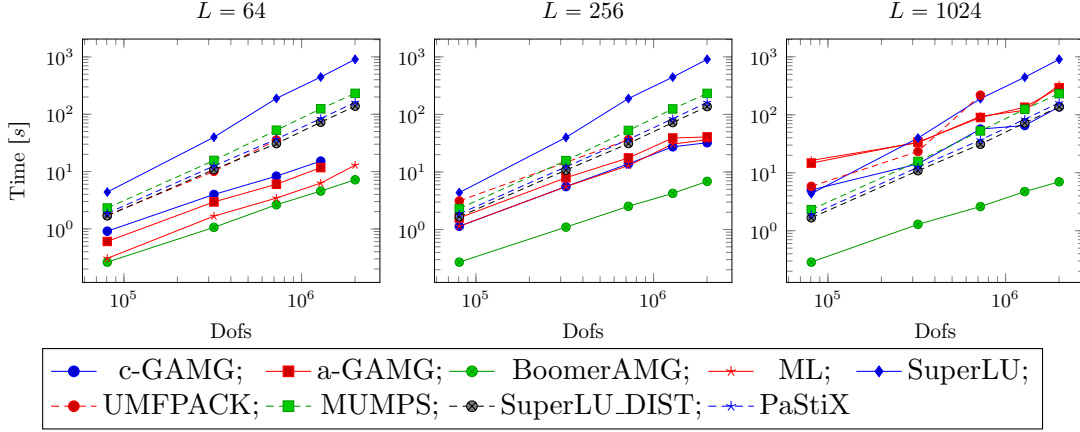


FIGURE 12. Time (for setup and solving) of direct and iterative solvers for the hexagonal meshes  $\text{hexa}_2$ ,  $\text{hexa}_4$ ,  $\text{hexa}_6$ ,  $\text{hexa}_8$  and  $\text{hexa}_{10}$  of Table 1 partitioned in  $L = 64, 256, 1024$  parts. Every elements of a part is assigned the same diffusion coefficient  $\rho = 10^\alpha$ , with  $\alpha \in [-5, 5]$ .

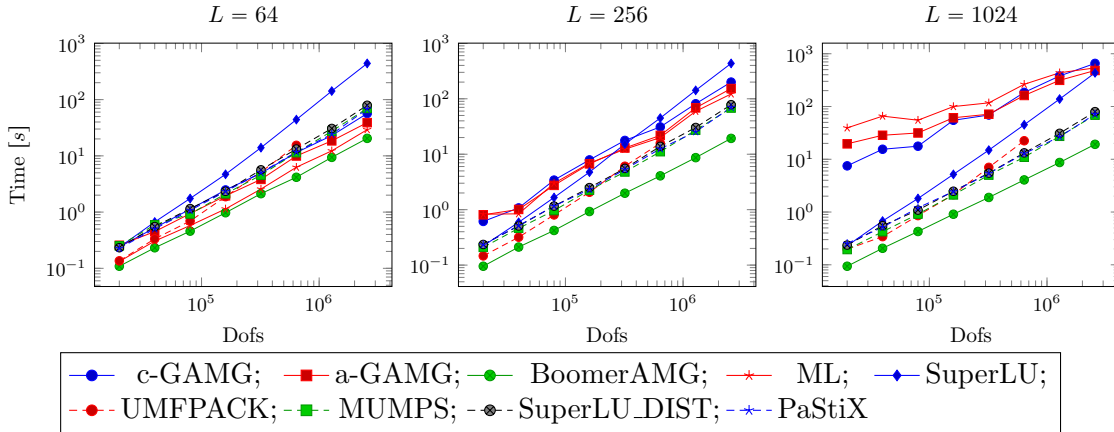


FIGURE 13. Time (for setup and solving) of direct and iterative solvers for the Voronoi meshes  $\text{vor}_3$ – $\text{vor}_{10}$  of Table 4 partitioned in  $L = 64, 256, 1024$  parts. Every elements of a part is assigned the same diffusion coefficient  $\rho = 10^\alpha$ , with  $\alpha \in [-5, 5]$ .

VEM discretization based on these meshes deserves further investigations that will be addressed in future works.

## REFERENCES

1. P. Amestoy, I. Duff, J. L'Excellent, and J. Koster, *A fully asynchronous multifrontal solver using distributed dynamic scheduling*, SIAM Journal on Matrix Analysis and Applications **23** (2001), no. 1, 15–41.
2. P. R. Amestoy, A. Guermouche, J. L'Excellent, and S. Pralet, *Hybrid scheduling for the parallel solution of linear systems*, Parallel Computing **32** (2006), no. 2, 136 – 156, Parallel Matrix Algorithms and Applications (PMAA04).
3. P. F. Antonietti, L. Beirão da Veiga, D. Mora, and M. Verani, *A stream virtual element formulation of the Stokes problem on polygonal meshes*, SIAM Journal on Numerical Analysis **52** (2014), no. 1, 386–404.
4. P. F. Antonietti, L. Beirão da Veiga, S. Scacchi, and M. Verani, *A  $C^1$  virtual element method for the Cahn-Hilliard equation with polygonal meshes*, SIAM Journal on Numerical Analysis **54** (2016), no. 1, 34–56.
5. P. F. Antonietti, L. Mascotto, and M. Verani, *A multigrid algorithm for the  $p$ -version of the virtual element method*, Math. Model. Numer. Anal. **52** (2018), no. 1, 337–364.

6. S. Balay, S. Abhyankar, M. F. Adams, J. Brown, P. Brune, K. Buschelman, L. Dalcin, A. Dener, V. Eijkhout, W. D. Gropp, D. Kaushik, M. G. Knepley, D. A. May, L. C. McInnes, R. T. Mills, T. Munson, K. Rupp, P. Sanan, B. F. Smith, S. Zampini, and H. Zhang, *PETSc Web page*, <http://www.mcs.anl.gov/petsc>, 2018.
7. ———, *PETSc users manual*, Tech. Report ANL-95/11 - Revision 3.9, Argonne National Laboratory, 2018.
8. L. Beirão da Veiga, F. Brezzi, A. Cangiani, G. Manzini, L. D. Marini, and A. Russo, *Basic principles of virtual element methods*, *Mathematical Models and Methods in Applied Sciences* **23** (2013), no. 1, 199–214.
9. L. Beirão da Veiga, F. Brezzi, and L. Marini, *Virtual elements for linear elasticity problems*, *SIAM Journal on Numerical Analysis* **51** (2013), no. 2, 794–812.
10. L. Beirão da Veiga, F. Brezzi, L. D. Marini, and A. Russo, *The Hitchhiker’s guide to the virtual element method*, *Mathematical Models and Methods in Applied Sciences* **24** (2014), no. 8, 1541–1573.
11. ———, *Mixed virtual element methods for general second order elliptic problems on polygonal meshes*, *ESAIM: M2AN* **50** (2016), no. 3, 727–747.
12. ———, *Virtual Element Method for general second-order elliptic problems on polygonal meshes*, *Mathematical Models and Methods in Applied Sciences* **26** (2016), no. 4, 729–750.
13. L. Beirão da Veiga, Lovadina C., and A. Russo, *Stability Analysis for the Virtual Element Method*, 2016, arXiv:1607.05988.
14. L. Beirão da Veiga, A. Chernov, L. Mascotto, and A. Russo, *Basic principles of hp virtual elements on quasiuniform meshes*, *Mathematical Models and Methods in Applied Sciences* **26** (2016), no. 8, 1567–1598.
15. L. Beirão da Veiga, C. Lovadina, and G. Vacca, *Divergence free virtual elements for the Stokes problem on polygonal meshes*, *ESAIM: M2AN* **51** (2017), no. 2, 509–535.
16. ———, *Virtual Elements for the Navier-Stokes problem on polygonal meshes*, arXiv e-prints (2017).
17. L. Beirão da Veiga, A. Russo, and G. Vacca, *The Virtual Element Method with curved edges*, ArXiv e-prints (2017).
18. M. F. Benedetto, S. Berrone, and S. Scialó, *A globally conforming method for solving flow in discrete fracture networks using the virtual element method*, *Finite Elements in Analysis and Design* **109** (2016), 23 – 36.
19. S. Berrone and A. Borio, *Orthogonal polynomials in badly shaped polygonal elements for the Virtual Element Method*, *Finite Elements in Analysis and Design* **129** (2017), 14–31.
20. S. Bertoluzza, M. Pennacchio, and D. Prada, *BDDC and FETI-DP for the virtual element method*, *Calcolo* **54** (2017), 1565–1593.
21. ———, *FETI-DP for the three-dimensional Virtual Element Method*, Tech. report, in preparation, 2018.
22. ———, *High order VEM on curved domains.*, Tech. report, IMATI-PV, 2018, arXiv:1811.04755.
23. V.E. Briggs, W.L.Henson and S.F. McCormick, *Why multigrid methods are so efficient.*, *Computing in Science and Engineering* **8** (2006), 12–22.
24. J.G. Calvo, *On the approximation of a virtual coarse space for domain decomposition methods in two dimensions*, *Math. Models Methods Appl. Sci.* **38** (2018), no. 7, 1267–1289.
25. ———, *An overlapping schwarz method for virtual element discretizations in two dimensions*, (available, november 2018).
26. A. Cleary, R. Falgout, V. Henson, J. Jones, T. Manteuffel, S. McCormick, G. Miranda, and J. Ruge, *Robustness and scalability of algebraic multigrid*, *SIAM Journal on Scientific Computing* **21** (2000), no. 5, 1886–1908.
27. L. Beirão da Veiga, C. Lovadina, and D. Mora, *A virtual element method for elastic and inelastic problems on polytope meshes*, *Computer Methods in Applied Mechanics and Engineering* **295** (2015), 327 – 346.
28. T. A. Davis, *Algorithm 832: Umfpack v4.3—an unsymmetric-pattern multifrontal method*, *ACM Trans. Math. Softw.* **30** (2004), no. 2, 196–199.
29. R. D. Falgout, J. E. Jones, and U. M. Yang, *The design and implementation of hypre, a library of parallel high performance preconditioners*, *Numerical Solution of Partial Differential Equations on Parallel Computers (Berlin, Heidelberg)*, Springer Berlin Heidelberg, 2006, pp. 267–294.
30. R.D. Falgout, *Introduction to algebraic multigrid*, *Computing in Science and Engineering* **8** (2006), 24–33.
31. M. Frittelli and I. Sgura, *Virtual Element Method for the Laplace-Beltrami equation on surfaces*, arXiv e-prints (2016).
32. A. L. Gain, C. Talischi, and G. H. Paulino, *On the virtual element method for three-dimensional linear elasticity problems on arbitrary polyhedral meshes*, *Computer Methods in Applied Mechanics and Engineering* **282** (2014), 132–160.
33. M.W. Gee, C.M. Siefert, J.J. Hu, R.S. Tuminaro, and M.G. Sala, *ML 5.0 smoothed aggregation user’s guide*, Tech. Report SAND2006-2649, Sandia National Laboratories, 2006.
34. G. H. Golub and C. F. Van Loan, *Matrix computations*, third ed., Johns Hopkins Studies in the Mathematical Sciences, Johns Hopkins University Press, Baltimore, MD, 1996.
35. P. Hnon, P. Ramet, and J. Roman, *Pastix: a high-performance parallel direct solver for sparse symmetric positive definite systems*, *Parallel Computing* **28** (2002), no. 2, 301 – 321.
36. G. Karypis, *METISc Web page*, <http://glaros.dtc.umn.edu/gkhome/metis/metis/overview>, 2015.

37. X. S. Li, *An overview of SuperLU: Algorithms, implementation, and user interface*, toms **31** (2005), no. 3, 302–325.
38. L. Mascotto, *Ill-conditioning in the virtual element method: Stabilizations and bases*, Numerical Methods for Partial Differential Equations **34** (2018), no. 4, 1258–1281.
39. L. Mascotto, L. Beirão da Veiga, A. Chernov, and A. Russo, *Exponential convergence of the hp Virtual Element Method with corner singularities*, Numer. Math. (2018), 138–581.
40. I. Perugia, P. Pietra, and A. Russo, *A plane wave virtual element method for the Helmholtz problem*, ESAIM: M2AN **50** (2016), no. 3, 783–808.
41. D. Prada, S. Bertoluzza, M. Pennacchio, and M. Livesu, *FETI-DP preconditioners for the Virtual Element Method on general 2D meshes*, in Numerical Mathematics and Advanced Applications - ENUMATH 2017, Springer International Publishing, to appear.
42. J.W. Ruge and K. Stüben., *Algebraic multigrid.*, Frontiers in Applied Mathematics, pp. 73–130, SIAM, 1987.
43. K. Stüben, *A review of algebraic multigrid*, Journal of Computational and Applied Mathematics **128** (2001), no. 1, 281 – 309.
44. C. Trottenberg, U. Oosterlee and A. Schüller, *Multigrid.*, Academic Press, 2001.
45. G. Vacca and L. Beirão da Veiga, *Virtual element methods for parabolic problems on polygonal meshes*, Numerical Methods for Partial Differential Equations **31** (2015), no. 6, 2110–2134.
46. P. Vaněk, J. Mandel, and M. Brezina, *Algebraic multigrid by smoothed aggregation for second and fourth order elliptic problems*, Computing **56** (1996), no. 3, 179–196.
47. U. M. Yang, *Parallel algebraic multigrid methods - high performance preconditioners*, Lecture Notes in Computational Science and Engineering, pp. 209–233, Springer, 2006.

IMATI “E. MAGENES”, CNR, PAVIA (ITALY)  
*E-mail address:* daniele.prada@imati.cnr.it

IMATI “E. MAGENES”, CNR, PAVIA (ITALY)  
*E-mail address:* micol.pennacchio@imati.cnr.it